irregular polyhedron (range of K(2)–Se distances, 3.694 (8)–3.253 (7) Å; av 3.470 Å). We note that examples of molecular uranium/chalcogenide complexes are sparce. A fully characterized homoleptic uranium thiolate has been recently reported.[6] Prior to this, most work has dealt with complexes of uranyl with various sulfur-containing ligands,[7] including a complex containing a single η^2-S_2^{2-}.[8,9]

The magnetic susceptibility of K_4USe_8 was measured as a function of temperature (5–250 K). Strong paramagnetic behavior, conforming to the Curie–Weiss law, is observed from approximately 120 K on up. Below this region, a transition is observed at approximately 90 K and is then followed by antiferromagnetic ordering which has a critical temperature of 65 K at the midpoint of a broad and shallow transition. The μ_{eff} at 300 K is 3.82 μ_B, consistent with an f^2 configuration where $L \neq 0$.[10] The exhibited paramagnetic behavior of the compound at high temperatures renders difficult any ^{77}Se NMR study of this compound. Antiferromagnetic transitions of various degrees have been reported for the uranium compounds MU_8Q_{17} (M = Cr, V, Co, Fe, Ni) by Noel and Troc,[11] although their data are complicated by the presence of M^{2+}. Neither K^+ nor Se_2^{2-} would contribute to any magnetic phenomenon, so, barring any impurity, we are observing behavior based solely on U^{4+}.

The solid-state far-IR spectrum of K_4US_8 shows three peaks: 261 cm^{-1}, which can be tentatively assigned to Se–Se stretching in the diselenides, and 167.6 and 153 cm^{-1}, which are presumably due to U–Se vibrations.

As mentioned before, K_4USe_8 is slowly soluble in DMF, and similar behavior has been found with ethylenediamine. The compound was insoluble in neat acetonitrile, even with the addition of $[(Bu)_4N]^+$; however, it was successfully dissolved in solutions of either 15C5 or 18C6 crown ethers or 2,2,2-cryptand in CH_3CN.

In all solvents the solutions of K_4USe_8 gave brown/yellow colors of various hues which were stable, by UV/vis, out to 3 days. The DMF and CH_3CN/complexant solutions gave similar UV/vis spectra: one broad plateau at 400–430 nm for DMF and at 390–430 nm for the CH_3CN/complexant. After decomposition the solutions revert to brown/green in color, and their UV/vis spectra show the features of a polyselenide solution (peaks at 400 and 640 nm for DMF 417 and 560 nm for CH_3CN). Such a decomposition takes place in all solvents tested upon exposure to air as well as simply upon standing, due to the high oxophilicity of U(IV), making distilled and degassed solvents a requirement. In ethylenediamine solutions of K_4USe_8, UV/vis shows peaks at 346, 404, 492, and 807 nm, while a polyselenide/ethylenediamine solution shows peaks at 408, 560, and 805 nm. Although clearly not a simple Se_x^{2-} solution, the presence of several peaks in the ethylenediamine solution indicates a significantly stronger solvent interaction with the anion than in either DMF or CH_3CN.

With preliminary indications that $[U(Se_2)_4]^{4-}$ may have appreciable stability in certain solvents, the possibility of using it as a starting material for further chemistry becomes intriguing. Potentially the $[U(Se_2)_4]^{4-}$ could be used as starting material for convenient entry into the unexplored U/Se chemistry or act as a ligand for other metals. The Se_2^{2-} units could present sites for facile redox chemistry and reactivity with organic molecules and organometallic compounds.

Acknowledgment. We thank Mr. Ju-Hsiou Liao for his help in X-ray data collection and the calculation for the sample's powder pattern. The NSF is gratefully acknowledged for support. Financial support is also acknowledged from the Center for Fundamental Materials Research at Michigan State University and the P. T. Barnum Memorial Circus Clown's Widows and Orphans Fund.

Supplementary Material Available: Tables of atomic coordinates, anisotropic thermal parameters, bond distances and angles of all atoms, and calculated and observed powder patterns (5 pages); listings of calculated and observed structure factors (6 pages). Ordering information is given on any current masthead page.

(6) Tatsumi, K.; Matsubara, I.; Inoui, Y.; Nakamura, A.; Cramer, R.; Tagosi, G.; Golen, J.; Gilje, J. *Inorg. Chem.* **1990**, *29*, 4928–4938.

(7) (a) Perry, D. L. *Inorg. Chim. Acta* **1978**, *48*, 117–124. (b) Perry, D. L.; Templeton, D. H.; Zalkin, A. *Inorg. Chem.* **1978**, *17*, 3699–3701. (c) Bowman, K.; Dori, Z. *J. Chem. Soc., Chem. Commun.* **1968**, 636. (d) Graziani, R.; Zarli, B.; Cassol, A.; Bombieri, G.; Forsellini, E.; Tondello, E. *Inorg. Chem.* **1970**, *9*, 2116–2124. (e) Bagnall, K. W.; Holah, D. G. *Nature (London)* **1967**, *215*, 623. (f) Bagnall, K. W.; Brown, D.; Holah, D. G. *J. Chem. Soc. A* **1968**, 1149–1153. (g) Bibler, J. P.; Karraker, D. G. *Inorg. Chem.* **1968**, *7*, 982–985. (h) Bombieri, G.; Croatto, U.; Forsellini, E.; Zarli, B.; Graziani, R. *J. Chem. Soc., Dalton Trans.* **1972**, 560–564. (i) Ryan, R. R.; Smith, B. F.; Ritchey, J. M. *Inorg. Chim. Acta* **1987**, *129*, 139–148.

(8) Perry, D.; Zalkin, A.; Ruben, H.; Templeton, D. H. *Inorg. Chem.* **1982**, *21*, 237–240.

(9) Many solid-state ternary uranium chalcogenides have been discovered over the last 20 years, and most commonly occurring are those of the types MUQ_3,[9a-c] MU_8Q_{17},[9b-e] and MU_2Q_5[9f] (where M = transition metal, or, in the case of MU_2Q_5, an alkali-earth, and Q = S, Se). All have been made with traditional high-temperature (800–1100 °C) synthetic methods, resulting in compounds with extended solid-state structures and monochalcogenides. (a) Noel, H.; Padiou, J.; Prigent, J. *C. R. Seances Acad. Sci. Ser. C* **1975**, *280*, 123–126. (b) Noel, H. *C. R. Seances Acad. Sci. Ser. C* **1973**, *277*, 463–464. (c) Noel, H. *C. R. Seances Acad. Sci. Ser. C* **1974**, *279*, 513–515. (d) Vovan, T.; Rodier, N. *C. R. Seances Acad. Sci. Ser. C* **1979**, *289*, 17–20. (e) Noel, H.; Potel, M.; Padiou, J. *Acta Crystallogr.* **1975**, *B31*, 2634–2637. (f) Brochu, R.; Padiou, J.; Prigent, J. *C. R. Seances Acad. Sci. Ser. C* **1972**, *274*, 959–961. (g) Noel, H.; Daoudi, J. *J. Solid State Chem.* **1985**, *60*, 131–134. (h) Noel, H.; Potel, M. *J. Less-Common Met.* **1985**, *113*, 11–15. (i) Noel, H. *J. Less-Common Met.* **1980**, *72*, 45–49.

(10) Figgis, B. N. In *Introduction to Ligand Fields*; Interscience Publishers: John Wiley and Sons: 1966.

(11) Noel, H.; Troc, R. *J. Solid State Chem.* **1979**, *27*, 123–135.

Crystal Structure and Preliminary Functional Analysis of the Cytochrome *c* Peroxidase His175Gln Proximal Ligand Mutant

Munirathin Sundaramoorthy, Kalidip Choudhury,† Steven L. Edwards, and Thomas L. Poulos*

Center for Advanced Research in Biotechnology of the Maryland Biotechnology Institute University of Maryland, Shady Grove 9600 Gudelsky Drive, Rockville, Maryland 20850 Department of Chemistry and Biochemistry University of Maryland, College Park, Maryland 20742

Received June 4, 1991

Cytochrome *c* peroxidase (CCP) catalyzes the peroxide-dependent oxidation of cytochrome *c* in the following multistep reaction:[1]

$$CCP + H_2O_2 \rightarrow CCP(Fe^{4+})^{\bullet}$$

$$CCP(Fe^{4+})^{\bullet} + 2cyt.c(Fe^{2+}) \rightarrow CCP + 2cyt.c(Fe^{3+})$$

H_2O_2 oxidizes CCP to an intermediate state termed compound I which consists of a ferryl (Fe^{4+}) iron and an amino acid(s) centered free radical denoted by the dot (•) in the above scheme. Central to the peroxidase mechanism are the invariant distal side residues, His52 and Arg48, which work in concert to stabilize the charge separation required in the heterolytic fission of the peroxide O–O bond.[2,3]

Less clear is the precise role of the proximal ligand. The function of the proximal ligand may be in regulating the iron redox potential, stabilizing the ferryl intermediate of compound I, assisting in cleavage of the peroxide O–O bond, and/or simply

* Author to whom correspondence should be addressed at CARB, 9600 Gudelsky Drive, Rockville, MD 20850.

† Department of Genetics, George Washington University, Washington, DC 20052.

(1) Yonetani, T. *Enzymes* **1976**, *13*, 345–361.

(2) Poulos, T. L.; Finzel, B. C. *Pept. Protein Rev.* **1984**, *4*, 115–171.

(3) Poulos, T. L. *Adv. Inorg. Biochem.* **1988**, *7*, 1–36.

0002-7863/91/1513-7755$02.50/0

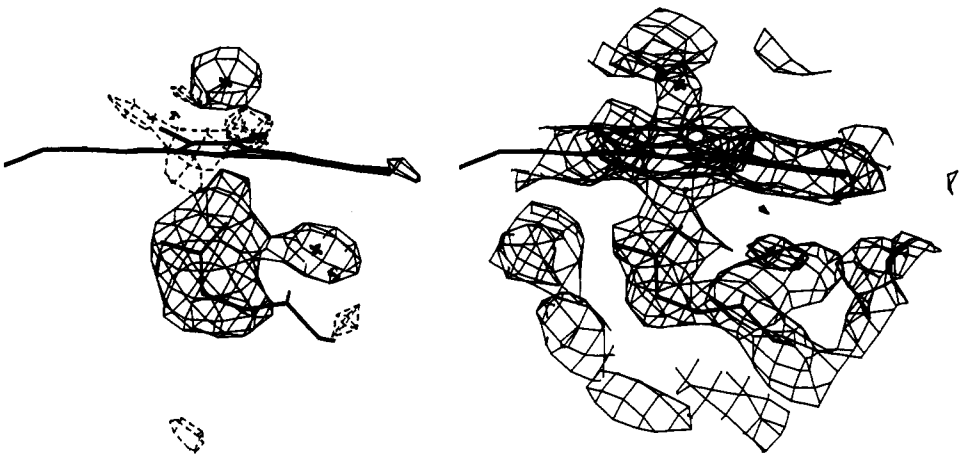

Figure 1. Left: The initial $F_o - F_c$ electron density difference maps contoured at $\pm 3\sigma$ where σ is the root-mean-square difference density. Negative contours are shown as dashed lines and positive contours as solid lines. The F_c phases were obtained from the wild-type refined structure except that the proximal ligand and the axial water molecule on the distal side of the heme were excluded from the structure factor calculation. Observed structure factors (F_o) were from the Gln175 data set. Right: The final $2F_o - F_c$ electron density map contoured at 1σ where σ is the root-mean-square electron density computed over an entire asymmetric unit. This is an "omit" map where the side chain of Gln175 and the two solvent molecules indicated by the small crosses were not included in the structure factor calculation. Note that the electron density between the distal solvent and iron is continuous, indicating that the iron may be hexacoordinate, although the visible absorption spectrum indicates a high-spin heme at pH 5.5. The Gln–iron and water–iron distances are about 2.2 and 2.3 Å, respectively.

Table I. Summary of Crystallographic Refinement[a]

	wild type	His175Gln
resolution range (Å)	10–2.0	10–2.0
data measured	27 686	23 448
data used ($I \geq 2\sigma$)	25 104	20 801
R factor[b]	0.17	0.20
rms deviation (Å) of atom pairs related through		
bonds	0.017	0.012
angles	0.024	0.023
dihedral angles	0.033	0.025
rms deviation (Å) of planar groups		
peptides	0.017	0.020
others	0.011	0.013
rms deviation (Å) of nonbonded contacts	0.181	0.179

[a] The software package PROFFT (Hendrickson, W. A.; Konnert, J. H. In *Computing in Crystallography*; Diamond, R., et al., Eds.; Indian Institute of Science: Bangalore, India, 1980; pp 13.1–13.23) was used for the refinement. [b] $R = \sum|F_o - F_c|/\sum F_o$. [c] The rms deviation of the final model represents the root-mean-square deviation of bond distances from expected values.

helping to hold the heme in place. In order to directly test the role of the proximal ligand, we have developed a recombinant *Escherichia coli* expression system for CCP.[4] This system has been used to convert the proximal ligand, His175, to Gln using site-directed mutagenesis. Both recombinant wild type and the His175Gln mutant were purified and crystallized.[5] The visible absorption spectrum of the mutant resembles a high-spin spectrum with a Soret maximum to 280 nm ratio of 1.25, which is comparable to the wild type enzyme ratio of 1.3, indicating that if the heme is hexacoordinate, it remains high-spin at pH 5.5. While the absorption spectrum at pH 5.5 is very similar to that of wild-type CCP, the Soret maximum has shifted from 408 nm to 404 nm.

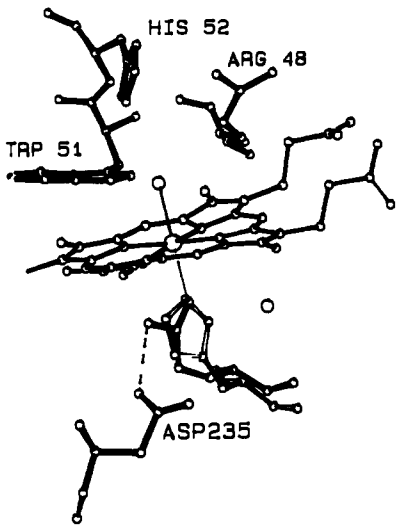

Figure 2. The mutant structure (solid bonds) superimposed on the wild-type structure (clear bonds). Dashed lines indicate hydrogen bonds, and the isolated spheres represent solvent molecules. The side-chain amide nitrogen of Gln175 forms a 2.9-Å hydrogen bond with Asp235 while the Gln175 side chain oxygen atom is 3.0 Å from the new water molecule situated in the proximal pocket for a second potential hydrogen bond. The Gln175–iron and water–iron distances are approximately 2.2 and 2.3Å, respectively.

A complete set of X-ray intensity data for each was obtained at 4 °C, and the structures were refined using restrained least-squares procedures[6] (Table I). The refined $2F_o - F_c$ (F_o = observed and F_c = calculated structure factors) electron density map is shown in Figure 1, and a superimposition of the mutant

(4) Darwish, K.; Li, H.; Poulos, T. L. *Protein Eng.*, in press.

(5) Purification of recombinant CCP was according to Fishel et al. (Fishel, L. A.; Villafranca, J. E.; Mauro, J. M.; Kraut, J. *Biochemistry* **1987**, *26*, 351–360) with slight modifications. Crystals were prepared from 2-methyl-2,4-pentanediol (MPD) according to Edwards and Poulos (Edwards, S. E.; Poulos, T. L. *J. Biol. Chem.* **1990**, *265*, 2588–2595) with the following modifications. Approximately 16 μL of 10 mg/mL CCP in 0.05 M potassium phosphate, pH 6.0, and 25% MPD was delivered into a 1-mm-wide X-ray capillary containing a small seed crystal. The seed crystal had been washed previously with decreasing concentrations of MPD beginning with 32.5% and ending with 27.5% in approximately 2.5% increments. The capillary was sealed in a sandwich box and vapor diffused against 35% MPD in the cold room (4 °C). Once the crystal had grown to sufficient size, the remainder of the surrounding solution was carefully removed, a mother liquor plug reintroduced above the crystal, and the capillary sealed with mineral oil. Mutant crystals proved to be temperature sensitive, so all data sets were obtained between 2 and 5 °C.

(6) Data sets were obtained from single crystals using a Siemens area detector system and a Rigaku rotating anode X-ray source. The temperature was regulated to between 2 and 5 °C by a stream of cooled air being blown over the crystal. Data were reduced and scaled using the XENGEN package of programs. For wild-type CCP, 99 558 observations scaled to give an R_{symm} = 0.063, while for the mutant, R_{symm} = 0.064 for 98 613 observation. $R_{symm} = \sum|I_i - \langle I_i\rangle|\sum I_i$ where I_i = intensity of the ith observation and $\langle I_i\rangle$ = mean intensity. For the wild-type data set, the data were 94% complete to 2.12 Å and 78% complete to 2.00 Å with the average intensity-to-background ratio = 2.0 at 2.0 Å. For the mutant, the data were 83% complete to 2.16 Å and 52% complete to 2.04 Å. The ratio of average intensity to background for the mutant was 2.05 at 2.04 Å.

and wild-type structures in the vicinity of the active site is shown in Figure 2. The results clearly demonstrate that the Gln side chain forms a bond with the iron, probably via the side-chain oxygen atom,[7] and that all structural changes are localized at the site of mutation.

Enzyme activities were determined by following the oxidation of reduced cytochrome *c* at pH 5.5 (0.1 M Tris-MES-acetate buffer) using excess horse heart cytochrome *c* (40 μM) and varying concentrations of H_2O_2. Kinetic constants were estimated from Eadie–Hofstee plots. For the wild-type enzyme, k_{cat} = 1463 s^{-1} and K_M = 6.7 μM, and for the Gln mutant, k_{cat} = 1585 s^{-1} and K_m = 58 μM. That it is possible to drastically change the coordination environment of the heme yet retain nearly full enzyme activity as estimated from the steady-state k_{cat} values is unexpected and calls into question the proposed roles of the proximal ligand. These results demonstrate that the precise nature of the proximal ligand is not critical in the rate-limiting step of the reaction, which very likely is electron transfer from cytochrome *c*.[8,9]

Acknowledgment. We thank Dr. Kamel Darwish for development of the CCP expression system and Dr. Matthew Mauro for invaluable insights on purification and analysis of mutant enzymes. This work was supported by NSF Grant DMB 8716316 and NIH Grant GM 42614.

Registry No. CCP, 9029-53-2; H_2O_2, 7722-84-1; His, 71-00-1; Gln, 56-85-9; Heme, 14875-96-8.

(7) We cannot be certain that the side-chain oxygen and not the side-chain nitrogen coordinates with the iron although an oxygen–iron bond seems more reasonable since formation of a nitrogen–iron bond would require a deprotonation of the amide nitrogen. Moreover, the 2.9-Å distance between the side chains of Gln175 and Asp235 would favor the amide nitrogen of Gln235 as a hydrogen-bond donor.

(8) Bosshard, H. R.; Anni, H.; Yonetani, T. In *Peroxidase in Chemistry and Biology*; Everse, J., Everse, K. E., Vol. II, pp 51–85. Grisham, M. B., Eds.; CRC Press: Boca Raton, FL, 1991; Vol. II, pp 51–84.

(9) Goddin, D. B.; Davidson, M. G.; Roe, J. A. S.; Mauk, A. G.; Smith, M. *Biochemistry* **1991**, *30*, 4953–4962.

Oxidative Conversion of a Mn(μ-OH)$_2$Mn to a Mn(μ-O)$_2$Mn Moiety. Synthesis and Molecular Structures of a (μ-Hydroxo)dimanganese(II,II) and (μ-Oxo)dimanganese(III,III) Complex with a Hindered N_3 Ligand

Nobumasa Kitajima,* Udai P. Singh,† Hironobu Amagai, Masahisa Osawa, and Yoshihiko Moro-oka*

Research Laboratory of Resources Utilization Tokyo Institute of Technology 4259 Nagatsuta, Midori-ku, Yokohama 227, Japan

Received February 1, 1991

A polymanganese site at the photosystem II oxygen-evolving center (PSII OEC) is known to be responsible for water oxidation to dioxygen. Despite current extensive studies, there is no consensus about the precise arrangement of the manganese atoms, their oxidation states, and the reaction mechanism.[1,2] Because the conversion of water to dioxygen is a four-electron oxidation with release of four protons, the oxidation is formally explicable in terms of the sequential transformation of two water molecules on the polymanganese site: $2H_2O \rightarrow 2OH^- \rightarrow 2O^{2-} \rightarrow O_2^{2-} \rightarrow O_2$. The proposed mechanisms[3,4] for OEC catalysis involve these elemental reaction steps, whereas they are based on a tetranuclear manganese structure for PSII OEC. Very recently, the first example of a (μ-peroxo)dimanganese complex was reported, and it was shown to release dioxygen.[5] This provides a solid chemical basis for the final step ($O_2^{2-} \rightarrow O_2$) in the hypothetical O_2 evolution mechanism. However, neither the oxidative conversion of a bis(μ-hydroxo) to a bis(μ-oxo) moiety nor O–O bond formation from a bis(μ-oxo) moiety on a polymanganese center has been demonstrated to date.

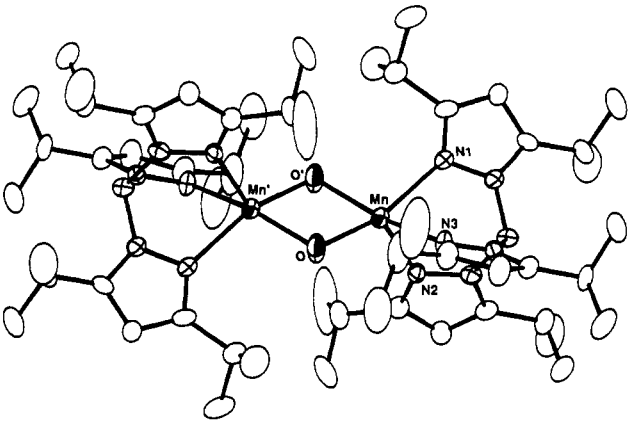

Figure 1. ORTEP view of [Mn(HB(3,5-iPr$_2$pz)$_3$)]$_2$(OH)$_2$ (**2**). The solvents of crystallization are omitted for clarity. Selected bond distances (Å) and angles (deg): Mn–O, 2.094 (4); Mn–O′, 2.089 (5); Mn–N1, 2.273 (5); Mn–N2, 2.204 (5); Mn–N3, 2.288 (5); Mn···Mn′, 3.314 (1); O···O′, 2.553 (7); Mn–O–Mn′, 104.8 (2).

A bis(μ-hydroxo) dinuclear Mn(II,II) complex was successfully prepared with a hindered tris(pyrazolyl)borate ligand in a manner similar to that applied for the synthesis of a bis(μ-hydroxo)copper(II,II) complex, [Cu(HB(3,5-iPr$_2$pz)$_3$)]$_2$(OH)$_2$.[6] The reaction of $MnCl_2$ with 1 equiv of KHB(3,5-iPr$_2$pz)$_3$ in the presence of excess (ca. 5 equiv) 3,5-iPr$_2$pz in a CH_2Cl_2/CH_3OH mixture afforded Mn(Cl)(3,5-iPr$_2$pz)(HB(3,5-iPr$_2$pz)$_3$) (**1**) as an air-stable, white solid. Treatment of a toluene solution of **1** with 1 N aqueous NaOH afforded [Mn(HB(3,5-iPr$_2$pz)$_3$)]$_2$(OH)$_2$ (**2**) in ca. 60% yield as a microcrystalline colorless solid.[8] Single crystals of **2**·6CH_2Cl_2 were obtained by slow recrystallization from CH_2Cl_2 at −20 °C. As shown in Figure 1, **2** has a dinuclear structure that sits on a crystallographically imposed center of symmetry.[9] Two hydroxo groups lie between the two manganese(II) ions with identical bond lengths (2.094 (4) and 2.089 (5) Å). Thus **2** is the first example of a dinuclear manganese complex in which the two manganese ions are bridged solely by hydroxo groups.[10] Previously, one example of a bis(μ-hydroxo)manganese(III,III) complex was reported.[11] However, the Mn–Mn separation (2.72

†UNESCO Research Fellow from Banaras Hindu University, India.

(1) (a) Brudvig, G. W. *Metal Clusters in Proteins*; Que, L., Jr., Ed.; ACS Symposium Series 372; American Chemical Society: Washington, DC, 1988; p 221. (b) Christou, G.; Vincent, J. B. *Ibid.*; p 238. (c) Wieghart, K. *Angew. Chem., Int. Ed. Engl.* **1989**, *28*, 1153.

(2) (a) Christou, G. *Acc. Chem. Res.* **1989**, *22*, 328. (b) Vincent, J. B.; Christou, G. *Adv. Inorg. Chem.* **1989**, *33*, 197.

(3) Brudvig, G. W.; Crabtree, R. H. *Proc. Natl. Acad. Sci. U.S.A.* **1986**, *83*, 4586.

(4) Christou, G.; Vincent, J. B. *Biochim. Biophys. Acta* **1988**, *895*, 259.

(5) Bossek, U.; Weyhermuller, T.; Wieghardt, K.; Nuber, B.; Weiss, J. *J. Am. Chem. Soc.* **1990**, *112*, 6387.

(6) (a) Kitajima, N.; Fujisawa, K.; Moro-oka, Y. *Inorg. Chem.* **1990**, *29*, 357. (b) Kitajima, N.; Fujisawa, K.; Fujimoto, C.; Moro-oka, Y.; Hashimoto, S.; Kitagawa, T.; Toriumi, K.; Tatsumi, K.; Nakamura, A. *J. Am. Chem. Soc.*, submitted for publication.

(7) Abbreviations: HB(3,5-iPr$_2$pz)$_3$, hydrotris(3,5-diisopropyl-1-pyrazolyl)borate; 3,5-iPr$_2$pz, 3,5-diisopropylpyrazole. Anal. Calcd for $C_{36}H_{61}N_8BMnCl$: C, 61.00; H, 8.61; N, 15.81; Cl, 5.00. Found: C, 60.88; H, 8.99; N, 15.61; Cl, 5.23. IR: ν(NH), 3292; ν(BH), 2528. The structure was established by X-ray crystallography, indicating a very distorted coordination geometry with a N_4Cl ligand donor set. The details will be described elsewhere.

(8) A satisfactory elemental analysis was obtained for **2** dried under vacuum. Anal. Calcd for $C_{54}H_{94}N_{12}O_2B_2Mn_2$: C, 60.03; H, 8.75; N, 15.65. Found: C, 60.42; H, 8.95; N, 15.54. IR: ν(OH) 3688; ν(BH) 2543 cm^{-1}.

(9) **2**·6CH_2Cl_2 ($C_{60}H_{106}N_{12}O_2B_2Cl_{12}Mn_2$; FW 1584.51) crystallized in the monoclinic space group $C2/c$ with a = 22.132 (4) Å, b = 13.386 (4) Å, c = 29.352 (7) Å, β = 110.56 (3)°, V = 8131 (3) Å^3, and Z = 4. Data collection ($2° < 2\theta < 45°$) was made at −50 °C to prevent the loss of CH_2Cl_2 molecules of crystallization. The refinement based on 2950 reflections ($F_o \geq 3\sigma F_o$) converged to final $R(R_w)$ values of 8.01% (7.73%).

(10) A dimanganese(II,II) complex having a Mn(OH)(OAc)$_2$Mn structure was reported: Wieghart, K.; Bossek, U.; Bonvoisin, J.; Beauvillain, P.; Girerd, J.-J.; Nuber, B.; Weiss, J.; Heinze, J. *Angew. Chem., Int. Ed. Engl.* **1986**, *25*, 1030.

(11) Maslen, H. S.; Waters, T. N. *J. Chem. Soc., Chem. Commun.* **1973**, 760.

0002-7863/91/1513-7757$02.50/0